High temperature neutron powder diffraction study of the Cu12Sb4S13 and Cu4Sn7S16 phases

P. Lemoine, Cédric Bourgès, Tristan Barbier, Vivian Nassif, Stéphane Cordier, Emmanuel Guilmeau

High temperature neutron powder diffraction study of the $Cu_{12}Sb_4S_{13}$ and $Cu_4Sn_7S_{16}$ phases

Pierric Lemoine[1*], Cédric Bourgès[2], Tristan Barbier[2], Vivian Nassif[3,4], Stéphane Cordier[1], Emmanuel Guilmeau[2]

[1] Institut des Sciences Chimiques de Rennes, UMR-CNRS 6226, 263 Avenue du Général Leclerc, CS 74205, 35042 Rennes Cedex, France

[2] Laboratoire CRISMAT, UMR-CNRS 6508, ENSICAEN, 6 Boulevard du Maréchal Juin, 14050 Caen Cedex 04, France

[3] CNRS Institut NEEL, F-38000 Grenoble, France

[4] Université de Grenoble Alpes, Institut NEEL, F-38000 Grenoble, France

* corresponding author: pierric.lemoine@univ-rennes1.fr

Abstract

Ternary copper-containing sulfides $Cu_{12}Sb_4S_{13}$ and $Cu_4Sn_7S_{16}$ have attracted considerable interest since few years due to their high-efficiency conversion as absorbers for solar energy and promising thermoelectric materials. We report therein on the decomposition study of $Cu_{12}Sb_4S_{13}$ and $Cu_4Sn_7S_{16}$ phases using high temperature *in situ* neutron powder diffraction. Our results obtained at a heating rate of 2.5 K/min indicate that: (i) $Cu_{12}Sb_4S_{13}$ decomposes above ≈ 792 K into Cu_3SbS_3, and (ii) $Cu_4Sn_7S_{16}$ decomposes above ≈ 891 K into Sn_2S_3 and a copper-rich sulfide phase of sphalerite ZnS-type structure with an assumed Cu_3SnS_4 stoichiometry. Both phase decompositions are associated to a sulfur volatilization. While the results on $Cu_{12}Sb_4S_{13}$ are in fair agreement with recent published data, the decomposition behavior of $Cu_4Sn_7S_{16}$ differs from other studies in terms of decomposition temperature, thermal stability and products of reaction. Finally, the crystal structure refinements from neutron powder diffraction data are reported and discussed for the $Cu_4Sn_7S_{16}$ and tetrahedrite $Cu_{12}Sb_4S_{13}$ phases at 300 K, and for the high temperature form of skinnerite Cu_3SbS_3 at 843 K.

Keywords: Sulfide material; Neutron powder diffraction; Thermal decomposition; Thermoelectric; Photovoltaic absorber

1. Introduction

In the past few years, several copper-containing sulfides have been reported as high-efficiency absorbers for solar energy conversion applications and promising thermoelectric materials [1-10]. Among them, ternary tetrahedrite $Cu_{12}Sb_4S_{13}$ and $Cu_4Sn_7S_{16}$ compounds have attracted considerable interest due to their complex crystal structures (Figure 1) characterized by an intrinsically low thermal conductivity [11-13].

$Cu_{12}Sb_4S_{13}$ crystallizes in the non-centrosymmetric cubic space group $I\bar{4}3m$ (No. 217) with copper atoms localized on 12d (¼, ½, 0) and 12e (x, 0, 0) crystallographic sites, antimony atoms localized on 8c (x, x, x) site, and sulfur atoms localized on 2a (0, 0, 0) and 24g (x, x, z) sites [14,15]. One of the complex feature of tetrahedrite crystal structure is related to copper atoms on the 12e site, which are in a trigonal plane environment formed by the sulfur atoms (two on the 24g site and one on the 2a site). This trigonal plane environment induces an important anisotropic atomic motion of the Cu

1

atoms perpendicularly to the trigonal plane defined by the sulfur atoms (Figure 1) [12,15-17]. It has been pointed out that this anisotropic atomic motion is also influenced by the Sb lone pair localized above and below the trigonal plane [18,19]. This structural feature favors phonon scattering leading to very low lattice thermal conductivity in tetrahedrites [18-21]. Another crystal structure description of tetrahedrite was proposed by Makovicky and Skinner [22]. Indeed, the authors have claimed that a split of the Cu 12e site into two lower symmetry 24g sites, statistically occupied, may described the anisotropic atomic motion as well [18,23,24]. Such structural description decreases the magnitude of the displacement parameters, and consequently improves the crystal structure refinement when isotropic (instead of anisotropic) displacement parameters are considered. Moreover, synthetic $Cu_{12}Sb_4S_{13}$ exhibits at low temperature a metal-semiconductor (also reported as a paramagnetic-nonmagnetic) transition around 85 K [11,20,25-27], which was recently associated to a concomitant structural transition from the well-known cubic structure to tetragonal structure [28,29]. Finally, synthetic $Cu_{12}Sb_4S_{13}$ sample evidences exsolution at low-temperature leading to Cu-poor and Cu-rich compounds. Consequently, the unit cell parameter ranges from 10.32 Å (Cu-poor) to 10.45 Å (Cu-rich) at room temperature [22,30,31].

$Cu_4Sn_7S_{16}$ crystallizes in the centrosymmetric trigonal space group $R\overline{3}m$ (No. 166) with copper atoms localized on the 3a (0, 0, 0) site and two 6c (0, 0, z) sites, tin atoms localized on the 3g (0, 0, ½) site and one 18h (x, -x, z) site, and sulfur atoms localized on two 6c (0, 0, z) sites and two 18h (x, -x, z) sites [32]. All crystallographic sites are fully occupied, excepted one of the 6c copper site (*i.e.* z ≈ 0.188), which is half occupied [32]. Similarly to the tetrahedrite structure, one of the complex feature of the crystal structure of $Cu_4Sn_7S_{16}$ is related to copper atoms on the 6c site (*i.e.* z ≈ 0.295), in a trigonal plane environment formed by sulfur atoms (all on the 18h (x ≈ 0.507, -x, z ≈ 0.376) site). This leads to an important anisotropic atomic motion of Cu atoms perpendicularly to the trigonal plane defined by sulfur atoms (Figure 1). Likewise, copper atoms on the 3a site are in an octahedral environment formed by sulfur atoms (all on the 18h (x ≈ 0.507, -x, z ≈ 0.376) site) and also evidence an anisotropic atomic motion of disk-like shape perpendicular to the *c*-axis (Figure 1). This former anisotropic atomic motion was described by Jemetio *et al.* [33] through a structural disorder considering a splitting of Cu 6c site atom (*i.e.* z ≈ 0.295) into two 6c sites (*i.e.* z ≈ 0.302 and z ≈ 0.290) statistically occupied. Finally, as in tetrahedrite, the aforementioned anisotropic atomic motions of copper atoms may contribute to the very low lattice thermal conductivity measured in $Cu_4Sn_7S_{16}$ [13].

While complex crystal structures of $Cu_{12}Sb_4S_{13}$ and $Cu_4Sn_7S_{16}$ compounds are now well-known, the thermal stability and phase decomposition of these materials remains ambiguous and not fully understood. The decomposition of pure synthetic tetrahedrite $Cu_{12}Sb_4S_{13}$ phase, studied from differential thermal analysis (DTA) and/or differential scanning calorimetry (DSC), has been examined by different authors [24,34-37]. Skinner *et al.* reported a phase decomposition of tetrahedrite around 816 K into famatinite Cu_3SbS_4, skinnerite Cu_3SbS_3, and a cation-disordered face-centered cubic phase [34]. Tatsuka and Morimoto mentioned the decomposition of the copper-poor tetrahedrite $Cu_{12.30}Sb_{4.05}S_{13}$ phase at about 816 K into famatinite Cu_3SbS_4, chalcostibite $CuSbS_2$ and the high-temperature form of skinnerite Cu_3SbS_3 [35]. Di Benedetto *et al.* attributed the endothermic effect on DTA curve starting at ≈ 813 K to the decomposition of pure copper synthetic tetrahedrite [36]. Braga *et al.* pointed out a phase decomposition of $Cu_{12}Sb_4S_{13}$ into Cu_3SbS_3 at 795 K [37], and more recently Barbier *et al.* shown that synthetic tetrahedrite $Cu_{12}Sb_4S_{13}$ phase decomposes into Cu_3SbS_3 (associated with sulfur volatilization) at a temperature starting from 791 K [24]. From X-ray powder diffraction data (XRPD), Barbier *et al.* highlighted that synthetic $Cu_{12}Sb_4S_{13}$ is stable up to 673 K and

decomposes at higher temperatures into Cu_3SbS_3 passing through $CuSbS_2$ as intermediate phase [24]. Finally, it could be mentioned that some studies relate on the breakdown below ≈ 634 K of skinnerite Cu_3SbS_3 into tetrahedrite $Cu_{12}Sb_4S_{13}$, antimony, and sometimes chalcostibite $CuSbS_2$ phases [30,34,38,39].

The ternary phase diagram Cu-Sn-S was studied totally or partially by several authors [40-43]. A state of the art of the ternary phases in this system can be found in reference [44]. According to the authors, different chemical formulas were assigned to describe the same crystalline phase. This is the case of $Cu_4Sn_7S_{16}$ for which chemical formulas ranging from $Cu_2Sn_3S_7$ to $Cu_2Sn_4S_9$ were reported. Among the publications on Cu-Sn-S ternary compounds, only few addressed on the melting or decomposition temperature of $Cu_4Sn_7S_{16}$, and the results obtained from DTA, DSC and XRPD experiments are strongly incoherent one to the others. Khanafer *et al.* mentioned the decomposition of cubic "$Cu_2Sn_4S_9$" (*i.e.* $Cu_4Sn_7S_{16}$) phase into "$Cu_4Sn_3S_8$" (which was discredited by Piskach *et al.* [42]) and SnS_2 at 938 K [40], Piskach *et al.* pointed out the formation of "$Cu_2Sn_4S_9$" through peritectoid reaction of Cu_2SnS_3 and SnS_2 at 943 K [42], and Fiechter *et al.* reported on the melting temperature at 1076 K of the wide stoichiometry range $Cu_2Sn_{3+x}S_{7+2x}$ ($0 \leq x \leq 1$) phase after three solid-solid phase transitions at 948 K, 958 K, and 1043 K [43].

Finally, the knowledge of the thermal phase stability/instability is fundamental for large scale applications, especially regarding thermoelectric materials. For this reason, we have investigated for the first time the temperature and phase decomposition of the ternary $Cu_{12}Sb_4S_{13}$ and $Cu_4Sn_7S_{16}$ compounds using *in situ* neutron powder diffraction (NPD) data recorded from room temperature up to 843 K and 1010 K, respectively. Moreover, we report, from long duration NPD data, on the crystal structure refinements of $Cu_{12}Sb_4S_{13}$ and $Cu_4Sn_7S_{16}$ compounds at 300 K and of the high temperature form of skinnerite Cu_3SbS_3 at 843 K.

2. Experimental methods

2.1. Synthesis

$Cu_{12}Sb_4S_{13}$ powder has been synthesized in a three-step process. Firstly, stoichiometric mixture of high purity powder elements (≥ 99.5 wt.%, Alfa Aesar) were sealed in evacuated silica tubes, heated up to 973 K for 3 h (rate of 100 K/h), then cooled down to 793 K (rate of 45 K/h), held for 25 h, before cooling to room temperature at the rate of 50 K/h. Resulting powder was then ground, sieved down to 200 μm, shaped into pellets using a hydraulic press, and sealed into an evacuated silica tube for a second annealing of 25 h at 793 K with heating and cooling rate of 100 K/h. The sample was finally crushed and sieved down to 200 μm before spark plasma sintering (SPS – FCT HPD 25) process at 793 K for 30 min (heating and cooling rate of 50 K/min and 200 K/min, respectively) under a pressure of 75 MPa using graphite dies of 15 mm diameter and a slight over pressure of argon (+20 hPa) to prevent oxidation and sulfur volatilization.

$Cu_4Sn_7S_{16}$ powder was synthesized in a two-step process. Firstly, stoichiometric mixture of high purity powder elements (Cu, S: ≥ 99.5 wt.%, Alfa Aesar; Sn: ≥ 99.9 wt.%, Merck) were sealed in evacuated silica tubes, heated up to 973 K at the rate of 100 K/h, held for 72 h and then cooled down to room temperature at the rate of 100 K/h. Secondly, the sample was ground, sieved down to 200 μm and densified by SPS (FCT HPD 25) at 973 K for 30 min (heating and cooling rate of 100 K/min) under a pressure of 64 MPa using graphite dies of 10 mm diameter and a slight over pressure of argon (+50 hPa) to prevent oxidation and sulfur volatilization.

The densified $Cu_{12}Sb_4S_{13}$ and $Cu_4Sn_7S_{16}$ pellets were crushed and sieved down to 200 μm prior to X-ray and neutron powder diffraction analyzes.

Remark: Similar synthesis processes were already performed to produce high density pellets of these materials. These pellets were then cut in several ingots used for thermoelectric properties measurements (*i.e.* Seebeck coefficient, electrical resistivity, thermal diffusivity). The thermoelectric properties of these materials, not reported here, are presented and discussed in references [24] and [13] for $Cu_{12}Sb_4S_{13}$ and $Cu_4Sn_7S_{16}$, respectively.

2.2. X-ray and neutron powder diffraction

The purity of the samples and the crystallographic structure of the phases were checked at room temperature by XRPD using a PANalytical X'Pert Pro diffractometer equipped with a Cu Kα X-ray tube. NPD experiments were carried out at the Institut Laue Langevin (ILL), Grenoble, France. The data were collected from room temperature up to 1010 K under dynamical secondary vacuum using the high-flux neutron two-axis powder diffractometer D1B (λ = 2.52 Å) equipped with a one-dimensional curved multidetector. The analysis of the diffraction patterns was performed by Rietveld profile refinement using the FullProf and WinPlotr software packages [45,46].

3. Results and discussion
3.1. $Cu_{12}Sb_4S_{13}$

NPD pattern recorded at T = 300 K on the $Cu_{12}Sb_4S_{13}$ sample (Figure 2) evidences the diffraction peaks of the cubic tetrahedrite $Cu_{12}Sb_4S_{13}$ phase (space group $I\bar{4}3m$, No. 217) as majority phase (81.5(8) wt.%) and of the tetragonal $Cu_{1.5}Sb_{0.5}S_2$ (CuFeS$_2$-type structure, space group $I\bar{4}2d$, No.122) and Cu_3SbS_4 (space group $I\bar{4}2m$, No. 121) phases (13.1(2) wt.% and 5.4(3) wt.%, respectively). These results are in fair agreement with previous X-ray diffraction analyses performed on similar sample [24]. Extra diffraction peaks observed around 75.6° and 90.1° on the neutron pattern are attributed to the thermocouple and were refined by pattern matching considering a simple *fcc* crystal structure of cell parameter $a \approx 3.56$ Å (space group $Fm\bar{3}m$, No. 225). The refinement of the tetrahedrite phase was performed using the crystal structure description proposed by Makovicky and Skinner [22]. Due to the limited number of observed diffraction peaks, only the profile peak-shape parameters, lattice parameters and the fractional atomic coordinates of the tetrahedrite phase were refined, while the fractional atomic coordinates of $Cu_{1.5}Sb_{0.5}S_2$ and Cu_3SbS_4 phases were fixed according to the structural data found in references [47,48]. The sites occupancies of the three phases were fixed to the theoretical values. The results of the crystal structure refinement of tetrahedrite phase are gathered in Table 1.

In order to carried out quantitative phase analysis of the $Cu_{12}Sb_4S_{13}$ phase decomposition under the same thermal conditions than those used by Barbier *et al.* during DSC and thermogravimetric analyses (TGA) [24], NPD patterns of 2 minutes were recorded continuously from 300 K up to 843 K at the rate of 2.5 K/min. The fractional atomic coordinates of the tetrahedrite phase refined at 300 K (Table 1) were used as fixed parameters in the refinement of the high temperature *in situ* neutron diffraction patterns.

NPD patterns recorded from 300 K up to 787 K show only a weak shift to the lower angles of the diffraction peaks of $Cu_{12}Sb_4S_{13}$ and $Cu_{1.5}Sb_{0.5}S_2$ phases in relation with the thermal expansion of their unit cells. The transformation of $Cu_{1.5}Sb_{0.5}S_2$ into $CuSbS_2$ (space group *Pnma*, No. 62 [49]) around 673

K noted by Barbier *et al.* [24] is not confirmed by NPD. Due to lower signal to noise ratio compared to the long duration 300 K neutron pattern, the existence of weak proportion of Cu_3SbS_4 as secondary phase is not confirmed at high temperature.

From T = 792 K, the intensity of the $Cu_{12}Sb_4S_{13}$ diffraction peaks decreases while concomitantly extra diffraction peaks appear (Figure 3). Those peaks are characteristic of the high temperature form of the orthorhombic skinnerite Cu_3SbS_3 phase (space group *Pnma*, No. 62) [50]. The diffraction peaks of the $Cu_{12}Sb_4S_{13}$ phase are not observed anymore above 836 K, while those of the $Cu_{1.5}Sb_{0.5}S_2$ phase (*i.e.* 47.6°, 55.4°, 55.8°, Figure 2) are observed up to 841 K (Figure 3). These results indicate that $Cu_{12}Sb_4S_{13}$ decomposes into Cu_3SbS_3 starting from 792 K up to 836 K (at the heating rate of 2.5 K/min), which is in good agreement with the results reported by Braga *et al.* [37] and Barbier *et al.* [24].

The unit cell parameters, occupancies of copper sites and fractional atomic coordinates (excepted those of Cu(4) and Cu(5) sites, which were fixed to those determined by Pfitzner at T = 493 K [50]) of the high temperature form of the orthorhombic skinnerite Cu_3SbS_3 phase were refined from long duration NPD pattern recorded at T = 843 K (Figure 4). The results are gathered in Table 2 and were used as fixed parameters in the refinement of the high temperature NPD patterns. The refined atomic coordinates are in fair agreement with those given by Pfitzner [50], while refined copper site occupancies evidence some differences, more especially concerning Cu(1), Cu(2), and Cu(5) sites. The refined occupation factors of copper sites lead to the stoichiometry $Cu_{2.99}SbS_3$ for the high temperature form of the skinnerite phase, which differs from the copper deficient stoichiometry $Cu_{2.922}SbS_3$ reported by Pfitzner [50].

Quantitative phase analysis data determined from Rietveld refinements of the NPD patterns recorded between 723 K and 841 K are displayed in Figure 5(a). They are compared with DSC and TGA results reported by Barbier *et al.* [24] (Figure 5(b)). The quantitative phase analysis highlights that the $Cu_{12}Sb_4S_{13}$ phase decomposes into Cu_3SbS_3 in two-step. Firstly, in the temperature range of 792 to 816 K, the majority of the $Cu_{12}Sb_4S_{13}$ phase decomposes into Cu_3SbS_3 and $Cu_{1.5}Sb_{0.5}S_2$ phases as expressed by the thermal evolution of the weight fraction of these phases (Figure 5(a)). Secondly, the weight fraction of the $Cu_{1.5}Sb_{0.5}S_2$ phase decreases above 816 K, while that of Cu_3SbS_3 continues to increase (Figure 5(a)). Considering that $CuSbS_2$ melts congruently around 826 K [34,37,51,52], we can conclude that the second step, between 816 K and 836 K, corresponds to the melting of $Cu_{1.5}Sb_{0.5}S_2$ associated with the end of the decomposition of $Cu_{12}Sb_4S_{13}$ into Cu_3SbS_3. It could be mentioned that the diffraction peaks of $Cu_{1.5}Sb_{0.5}S_2$ have totally disappeared after a dwell time of 8 minutes at 843 K.

The quantitative phase analysis results and starting/ending temperatures of phase decomposition determined from NPD are in excellent agreement with the DSC results (Figure 5). Moreover, considering that the transformation of $Cu_{12}Sb_4S_{13}$ into Cu_3SbS_3 requires sulfur loss, the mass loss observed on the thermogravimetric curve (Figure 5(b)) can then be attributed to a sulfur volatilization coming from the $Cu_{12}Sb_4S_{13}$ phase decomposition. The present results corroborate the study of Barbier *et al.* performed with the same thermal treatment [24]. Finally, the origin of the weak inflection around 835 K on the DSC curve (Figure 5(b)) can be attributed to the end of the $Cu_{12}Sb_4S_{13}$ phase decomposition (Figure 5(a)).

The phase stability of $Cu_{12}Sb_4S_{13}$ is then confirmed up to ≈ 792 K. It is important to note that considering the heating rate of 2.5 K/min, this value is probably slightly overestimated. It implies that

the physical properties of the $Cu_{12}Sb_4S_{13}$ tetrahedrite phase should evolve, and consequently have to be considered carefully, if the material is exposed at a temperature higher or close to 790 K. For higher temperature applications, Ni to Cu substituted tetrahedrite samples can be privileged. Indeed, it was demonstrated by Barbier *et al.* [24] that Ni for Cu substitution enhances the phase stability of the tetrahedrite phase at high temperature. *In situ* neutron powder diffraction performed on $Cu_{10.4}Ni_{1.6}Sb_4S_{13}$ sample up to 843 K (heating rate of 2.5 K/min) evidences the absence of structural modifications (data not shown) and then confirm the beneficial effect of Ni substitution on the thermal stability of tetrahedrite phase.

3.2. $Cu_4Sn_7S_{16}$

NPD pattern recorded at T = 300 K on the $Cu_4Sn_7S_{16}$ sample (Figure 6) evidences only the diffraction peaks of the rhombohedral $Cu_4Sn_7S_{16}$ compound (space group $R\overline{3}m$, No. 166). The refinement has been performed considering the crystal structure description reported by Jemetio *et al.* [33], where Cu(2) atoms are statistically distributed on two 6*c* sites instead of only one 6*c* site as reported by Chen *et al.* [32]. The lattice parameters and the fractional atomic coordinates were refined while the site occupancies were fixed to those reported by Jemetio *et al.* [33]. The results are gathered in Table 3.

In order to perform *in situ* quantitative phase analysis of the $Cu_4Sn_7S_{16}$ phase decomposition, NPD patterns of 2 minutes were recorded continuously from 300 K up to 823 K at the rate of 20 K/min and then from 823 K up to 1010 K at the rate of 2.5 K/min. The fractional atomic coordinates refined at 300 K (Table 3) were used as fixed parameters in the refinement of the high temperature NPD patterns. Intensities of the diffraction peaks are constant between 300 K and 823 K, indicating the absence of crystal structure evolution on this temperature range. Therefore, only NPD patterns recorded from 823 K to 1010 K have been carefully analyzed.

The neutron thermogram of $Cu_4Sn_7S_{16}$ recorded between 823 K and 1010 K is shown in Figure 7(a). The temperature dependence of the independent (2 0 8) reflection (2θ = 57.4°) intensity of $Cu_4Sn_7S_{16}$ and of one diffraction peak (2θ = 81.2°) corresponding to a secondary phase is displayed in Figure 7(b). Up to 891 K, the NPD patterns evidence only the diffraction peaks of the $Cu_4Sn_7S_{16}$ phase, indicating that this phase is chemically stable up to this temperature. Above 891 K, extra diffraction peaks appear on the NPD patterns, and concomitantly, the intensity of the diffraction peaks of $Cu_4Sn_7S_{16}$ decreases. These results indicate that $Cu_4Sn_7S_{16}$ starts to decompose above 891 K at the heating rate of 2.5 K/min. The extra diffraction peaks related to the thermal decomposition of $Cu_4Sn_7S_{16}$ are characteristic of the Sn_2S_3 phase (space group *Pnma*, No. 62) [53] and of a copper-rich sulfide phase for which several crystal structure descriptions can be considered (see below). Above 960 K, the intensity of all of the diffraction peaks strongly decreases (Figure 7). Above 976 K the diffraction peaks of Sn_2S_3 are no more observed and from 990 K only the signal of the copper-rich sulfide phase is still detected. It could be related with the experimental observation (after cooling) of a reaction between the sample and the vanadium sample holder. From thermodynamic study of the S-Sn system, Lindwall *et al.* [54] reported about the decrease of the melting temperature of Sn_2S_3 with the decrease of the gas pressure. Taking into account that the measurement was performed under dynamical secondary vacuum, the reaction of the sample with vanadium is likely the result of the melting of Sn_2S_3 at a lower temperature than the expected one (*i.e.* T_m = 1031 K [54]). Moreover, Lindwall *et al.* [54] concluded that, due to its lower sulfur content, Sn_2S_3 is more thermally stable than SnS_2 at low pressure (*i.e.* < 1 bar), which is confirmed by our neutron powder diffraction results.

In order to determine more accurately the crystal structure of the copper-rich sulfide phase, Rietveld refinements have been performed on the NPD pattern recorded at 990 K by considering: (i) the monoclinic form of mohite Cu_2SnS_3 (space group Cc, No. 9) [40,55,56], (ii) the tetragonal form of Cu_2SnS_3 in the stannite Cu_2FeSnS_4-type structure (space group $I\bar{4}2m$, No. 121) [32], (iii) the tetragonal form of kuramite Cu_3SnS_4 in the stannite Cu_2FeSnS_4-type structure (space group $I\bar{4}2m$, No. 121) reported with a sulfur deficiency by Goto et $al.$ [57], (iv) the cubic form of Cu_2SnS_3 in the sphalerite ZnS-type structure (space group $F\bar{4}3m$, No. 216) [58], and (v) the cubic form of kuramite Cu_3SnS_4 in the sphalerite ZnS-type structure (space group $F\bar{4}3m$, No. 216) [59]. All of these crystal structures lead to equivalent quality of refinements. It is important to note that the crystal structure of the high-temperature form of digenite $Cu_{2-\alpha}S$ (space group: $F\bar{4}3m$, No. 216 or $Fm\bar{3}m$, No. 225), does not fit correctly the intensity of the observed diffraction peaks.

According to Di Benedetto et $al.$ [59], the tetragonal crystal structure of Cu_3SnS_4 (iii) generates reflections which are absent in the experimental neutron pattern ($i.e.$ (0 0 2), (1 0 1), (1 1 0)), but consistent with the cubic sphalerite-type structure (iv) and (v). Similar interpretation can be done with the monoclinic form (i) and tetragonal form (ii) of mohite Cu_2SnS_3. Hence, we can concluded that the copper-rich sulfide phase detected by neutron powder diffraction crystallizes in the cubic sphalerite-type structure (space group $F\bar{4}3m$) with refined cell parameter a = 5.483(2) Å at 990 K. To this point, the cubic form of mohite Cu_2SnS_3 (iv) and the cubic form of kuramite Cu_3SnS_4 (v) cannot be distinguished. However, considering that the cubic form of Cu_2SnS_3 (iv) is known to be stable above 1053 K [32,56], we can assume that, at 990 K, the copper-rich sulfide phase is the cubic form of Cu_3SnS_4 (v). Refinement of the 990 K neutron pattern considering the Cu_3SnS_4 stoichiometry is displayed in Figure 8.

In the sphalerite ZnS-type structure, the $4a$ (0, 0, 0) and $4c$ (¼, ¼, ¼) crystallographic sites are fully occupied by zinc and sulfur atoms, respectively. Thus, in the cubic form of kuramite Cu_3SnS_4, it implies that copper and tin atoms are randomly distributed on the $4a$ (0, 0, 0) site [59]. From magnetic characterization of the cubic form of kuramite nanopowders, Di Benedetto et $al.$ concluded to the expected stoichiometry of Cu_3SnS_4 [59]. In our case, a different Cu/Sn ratio is not excluded. Unfortunately, the quality of the neutron diffraction data recorded at 990 K is too weak to allow the refinement of the Cu/Sn ratio. For this reason, the exact chemical composition of the present sphalerite-type phase cannot be confirmed. Nevertheless, the impact on NPD refinement of a different Cu/Sn ratio is very weak, and the cubic form of kuramite Cu_3SnS_4 well describes the copper-rich sulfide phase.

Due to the reaction of the sample with the vanadium sample holder above 960 K, the quantitative phase analysis has been done from Rietveld refinement of the NPD patterns recorded between 852 K and 960 K. The results, shown in Figure 9, indicate that $Cu_4Sn_7S_{16}$ decomposes progressively above 891 K into Sn_2S_3 (space group $Pnma$, No. 62) [53] and a copper-rich sulfide phase of sphalerite ZnS-type structure (space group $F\bar{4}3m$, No. 216) assumed to have the stoichiometry Cu_3SnS_4 [59]. Considering that the measurements have been done at a heating rate of 2.5 K/min, the starting temperature of decomposition of $Cu_4Sn_7S_{16}$, comprised between 891 K and 896 K, is probably slightly overestimated. Finally, during this decomposition, sulfur volatilization is assumed in order to balance the stoichiometry, leading to the following reaction: $Cu_4Sn_7S_{16} \rightarrow$ 17/6 Sn_2S_3 + 4/3 Cu_3SnS_4 + 13/6x $S_{x(g)}$ (2 ≤ x ≤ 10).

Our results highlight that the decomposition of $Cu_4Sn_7S_{16}$ starts at a temperature ≈ 40 K lower than that reported up to now [40,42], and leads to the formation of Sn_2S_3 instead of SnS_2 [40,42]. Moreover our results indicate the formation of a cubic sphalerite ZnS-type structure with assumed Cu_3SnS_4 stoichiometry. As already mentioned, the Cu_2SnS_3 stoichiometry reported by Piskach et $al.$

7

[42] is however not excluded. Finally, our results are in deep disagreement with those published by Fiechter *et al.* [43], where three solid-solid phase transitions of the $Cu_2Sn_{3+x}S_{7+2x}$ ($0 \leq x \leq 1$) phase are reported at 948 K, 958 K, and 1043 K, followed by the melting of the phase at 1076 K.

These results highlight that the $Cu_4Sn_7S_{16}$ phase is stable up to $\approx$ 891 K. Consequently, if the material is exposed at a temperature higher or close to 890 K the physical properties of the $Cu_4Sn_7S_{16}$ phase should evolve, and then have to be considered carefully.

4. Conclusion

High resolution neutron powder diffraction data collected from room temperature up to 1010 K under dynamical secondary vacuum have been analyzed to determine the temperatures and chemical reactions associated with the phase decompositions at the heating rate of 2.5 K/min of the ternary $Cu_{12}Sb_4S_{13}$ tetrahedrite and $Cu_4Sn_7S_{16}$ phases. The results highlight that (i) $Cu_{12}Sb_4S_{13}$ tetrahedrite phase decomposes above 792 K (and up to 836 K) into the high temperature form of skinnerite Cu_3SbS_3 and $Cu_{1.5}Sb_{0.5}S_2$ phases, this later being instable above 816 K, and (ii) $Cu_4Sn_7S_{16}$ phase decomposes above 891 K into Sn_2S_3 and a cubic phase of sphalerite ZnS-type structure. During these phase decompositions, sulfur volatilization likely occurs in order to balance the overall stoichiometry. While, high temperature *in situ* neutron powder diffraction results obtained on $Cu_{12}Sb_4S_{13}$ tetrahedrite phase confirm previous conclusions reported by Barbier *et al.* [24], the data obtained on $Cu_4Sn_7S_{16}$ lead to significant differences in comparison to previous thermal studies. In particular the temperature of decomposition is $\approx$ 40 K lower than previously reported values [40,42]. Our results also indicate that the interpretations of the data related to the $Cu_2Sn_{3+x}S_{7+2x}$ ($0 \leq x \leq 1$) phase in the pseudobinary $Cu_2S - SnS_2$ phase diagram proposed by Fiechter *et al.* [43] are not fully correct. These updates on the thermal stability/instability of the ternary $Cu_{12}Sb_4S_{13}$ and $Cu_4Sn_7S_{16}$ phases are new information that scientific community have to take into account for potential high temperature applications, especially in thermoelectricity.

References

[1] Y. Zhao, C. Burda, Energy Environ. Sci. 5 (2012) 5564-5576.

[2] K. Ramasamy, M.A. Malik, N. Revaprasadu, P. O'Brien, Chem. Mater. 25 (2013) 3551-3569.

[3] P. Zawadzki, L.L. Baranowski, H. Peng, E.S. Toberer, D.S. Ginley, W. Tumas, A. Zakutayev, S. Lany, Appl. Phys. Lett. 103 (2013) 253902.

[4] A.P. Gonçalves, C. Godart, Eur. Phys. J. B 87 (2014) 42.

[5] P. Jood, M. Ohta, Materials 8 (2015) 1124-1149.

[6] R. Chetty, A. Bali, R.C. Mallik, J. Mater. Chem. C 3 (2015) 12364-12378.

[7] S. Hébert, D. Berthebaud, R. Daou, Y. Bréard, D. Pelloquin, E. Guilmeau, F. Gascoin, O. Lebedev, A. Maignan, J. Phys.: Condens. Matter 28 (2016) 013001.

[8] P. Qiu, X. Shi, L. Chen, Energy Storage Mater. 3 (2016) 85-97.

[9] K. Suekuni, T. Takabatake, APL Mater. 4 (2016) 104503.

[10] Z.-H. Ge, L.-D. Zhao, D. Wu, X. Liu, B.-P. Zhang, J.-F. Li, J. He, Materials Today 19 (2016) 227-239.

[11] K. Suekuni, K. Tsuruta, T. Ariga, M. Koyano, Appl. Phys. Express 5 (2012) 051201.

[12] K. Suekuni, K. Tsuruta, M. Kunii, H. Nishiate, E. Nishibori, S. Maki, M. Ohta, A. Yamamoto, M. Koyano, J. Appl. Phys. 113 (2013) 043712.

[13] C. Bourgès, P. Lemoine, O.I. Lebedev, R. Daou, V. Hardy, B. Malaman, E. Guilmeau, Acta Mater. 97 (2015) 180-190.

[14] L. Pauling, E.W. Neuman, Z. Kristallogr. 88 (1934) 54-62.

[15] B.J. Wuensch, Z. Kristallogr. 119 (1964) 437-453.

[16] A. Pfitzner, M. Evain, V. Petricek, Acta Cryst. B 53 (1997) 337-345.

[17] Y. Bouyrie, C. Candolfi, V. Ohorodniichuk, B. Malaman, A. Dauscher, J. Tobola, B. Lenoir, J. Mater. Chem. C 3 (2015) 10476-10487.

[18] W. Lai, Y. Wang, D.T. Morelli, X. Lu, Adv. Funct. Mater. 25 (2015) 3648-3657.

[19] Y. Bouyrie, C. Candolfi, S. Pailhès, M.M. Koza, B. Malaman, A. Dauscher, J. Tobola, O. Boisron, L. Saviot, B. Lenoir, Phys. Chem. Chem. Phys. 17 (2015) 19751-19758.

[20] E. Lara-Curzio, A.F. May, O. Delaire, M.A. McGuire, X. Lu, C.-Y. Liu, E.D. Case, D.T. Morelli, J. Appl. Phys. 115 (2014) 193515.

[21] K. Suekuni, H.I. Tanaka, F.S. Kim, K. Umeo, T. Takabatake, J. Phys. Soc. Jpn. 84 (2015) 103601.

[22] E. Makovicky, B.J. Skinner, Can. Mineral. 17 (1979) 619-634.

[23] J.W. Andreasen, E. Makovicky, B. Lebech, S.K. Moller, Phys. Chem. Minerals 35 (2008) 447-454.

[24] T. Barbier, P. Lemoine, S. Gascoin, O.I. Lebedev, A. Kaltzoglou, P. Vaqueiro, A.V. Powell, R.I. Smith, E. Guilmeau, J. Alloys Compd. 634 (2015) 253-262.

[25] F. Di Benedetto, G.P. Bernardini, C. Cipriani, C. Emiliani, D. Gatteschi, M. Romanelli, Phys. Chem. Minerals 32 (2005) 155-164.

[26] K. Suekuni, Y. Tomizawa, T. Ozaki, M. Koyano, J. Appl. Phys. 115 (2014) 143702.

[27] S. Kitagawa, T. Sekiya, S. Araki, T.C. Kobayashi, K. Ishida, T. Kambe, T. Kimura, N. Nishimoto, K. Kudo, M. Nohara, J. Phys. Soc. Jpn. 84 (2015) 093701.

[28] H.I. Tanaka, K. Suekuni, K. Umeo, T. Nagasaki, H. Sato, G. Kutluk, E. Nishibori, H. Kasai, T. Takabatake, J. Phys. Soc. Jpn. 85 (2016) 014703.

[29] A.F. May, O. Delaire, J.L. Niedziela, E. Lara-Curzio, M.A. Susner, D.L. Abernathy, M. Kirkham, M.A. McGuire, Phys. Rev. B 93 (2016) 064104.

[30] K. Tatsuka, N. Morimoto, Am. Mineral. 58 (1973) 425-434.

[31] E. Makovicky, B.J. Skinner, Can. Mineral. 16 (1978) 611-623.

[32] X.A. Chen, H. Wada, A. Sato, M. Mieno, J. Solid State Chem. 139 (1998) 144-151.

[33] J.P.F. Jemetio, P. Zhou, H. Kleinke, J. Alloys Compd. 417 (2006) 55-59.

[34] B.J. Skinner, F.D. Luce, E. Makovicky, Econ. Geol. 67 (1972) 924-938.

[35] K. Tatsuka, N. Morimoto, Am. Mineral. 62 (1977) 1101-1109.

[36] F. Di Benedetto, G.P. Bernardini, D. Borrini, C. Emiliani, C. Cipriani, C. Danti, A. Caneshi, D. Gatteschi, M. Romanelli, Can. Mineral. 40 (2002) 837-847.

[37] M.H. Braga, J.A. Ferreira, C. Lopes, L.F. Malheiros, Mater. Sci. Forum 587-588 (2008) 435-439.

[38] L.T. Bryndzia, O.J. Kleppa, Am. Mineral. 73 (1988) 707-713.

[39] L.T. Bryndzia, A.M. Davis, Am. Mineral. 74 (1989) 236-242.

[40] M. Khanafer, J. Rivet, J. Flahaut, Bull. de la Société Chimique de France 12 (1974) 2670-2676.

[41] D. Wu, C.R. Knowles, L.L.Y. Chang, Mineral. Mag. 50 (1986) 323-325.

[42] L.V. Piskach, O.V. Parasyuk, I.D. Olekseyuk, J. Alloys Compd. 279 (1998) 142-152.

[43] S. Fiechter, M. Martinez, G. Schmidt, W. Henrion, Y. Tomm, J. Phys. Chem. Solids 64 (2003) 1859-1862.

[44] A. Giaccherini, G. Montegrossi, F. Di Benedetto, Minerals 6 (2016) 79.

[45] J. Rodriguez-Carvajal, Physica B 192 (1993) 55-59.

[46] T. Roisnel, J. Rodriguez-Carvajal, Mater. Sci. Forum 378-381 (2001) 118-123.

[47] S.R. Hall, J.M. Stewart, Acta Cryst., B 29 (1973) 579-585.

[48] A. Pfitzner, S. Reiser, Z. Kristallogr. 217 (2002) 51-54.

[49] A. Kyono, M. Kimata, Am. Mineral. 90 (2005) 162-165.

[50] A. Pfitzner, Z. Kristallogr. 213 (1998) 228-236.

[51] A. Wachtel, A. Noreika, J. Electron. Mater. 9 (1980) 281-297.

[52] B.V. Korzun, A.N. Gavrilenko, A.A. Fadzeyeva, O.V. Ignatenko, I.I. Maroz, V.R. Sobol, M. Rusu, R. Klenk, C. Merschjann, Th. Schedel-Niedrig, M.Ch. Lux-Steiner, Cryst. Res. Technol. 48 (2013) 641-648.

[53] R. Kniep, D. Mootz, U. Severin, H. Wunderlich, Acta Cryst. B 38 (1982) 2022-2023.

[54] G. Lindwall, S.L. Shang, N.R. Kelly, T. Anderson, Z.-K. Liu, Sol. Energy 125 (2016) 314-323.

[55] L.M. de Chalbaud, J.M. Delgado, V. Sagredo, Inst. Phys. Conf. Ser. No 152: Section A: Crystal Growth and Characterization (1998), 151-154.

[56] M. Onoda, X.A. Chen, A. Sato, H. Wada, Mater. Res. Bull. 35 (2000) 1563-1570.

[57] Y. Goto, F. Naito, R. Sato, K. Yoshiyasu, T. Itoh, Y. Kamihara, M. Matoba, Inorg. Chem. 52 (2013) 9861-9866.

[58] J. Rivet, J. Flahaut, P. Laruelle, C. R. Hebd. Seances Acad. Sci. 157 (1963) 161-164.

[59] F. Di Benedetto, D. Borrini, A. Caneschi, G. Fornaciai, M. Innocenti, A. Lavacchi, C.A. Massa, G. Montegrossi, W. Oberhauser, L.A. Pardi, M. Romanelli, Phys. Chem. Minerals 38 (2011) 483-490.

Figure captions

Figure 1: Crystal structure representations of $Cu_{12}Sb_4S_{13}$ and $Cu_4Sn_7S_{16}$.

Figure 2: Refinement of the neutron diffraction pattern of $Cu_{12}Sb_4S_{13}$ recorded at 300 K (λ = 2.52 Å).

Figure 3: Neutron diffraction patterns of $Cu_{12}Sb_4S_{13}$ sample recorded between 743 K and 841 K (λ = 2.52 Å).

Figure 4: Refinement of the neutron diffraction pattern of Cu_3SbS_3 recorded at 843 K (λ = 2.52 Å).

Figure 5: Quantitative phase analysis from Rietveld refinement of the NPD patterns (a) and DSC and TGA data (b) from ref. [24] of $Cu_{12}Sb_4S_{13}$ phase decomposition.

Figure 6: Refinement of the neutron diffraction pattern of $Cu_4Sn_7S_{16}$ recorded at 300 K (λ = 2.52 Å).

Figure 7: (a) Neutron thermogram of $Cu_4Sn_7S_{16}$ sample recorded between 823 K and 1010 K and (b) thermal evolution of the intensity of the independent (2 0 8) reflection of $Cu_4Sn_7S_{16}$ and of the (2 2 0) reflection of the cubic form of Cu_3SnS_4.

Figure 8: Refinement of the neutron diffraction pattern recorded at 300 K (λ = 2.52 Å) considering the sphalerite-type structure form of kuramite Cu_3SnS_4.

Figure 9: Quantitative phase analysis of the $Cu_4Sn_7S_{16}$ phase decomposition at the heating rate of 2.5 K/min from Rietveld refinement of the neutron diffraction patterns.

Table 1: Crystallographic parameters of $Cu_{12}Sb_4S_{13}$ deduced from Rietveld refinement of neutron powder diffraction pattern recorded at 300K.

$Cu_{12}Sb_4S_{13}$	$I\bar{4}3m$ a = 10.308(1) Å				
	Site	x	y	z	Occ.
Cu(1)	12*d*	¼	½	0	1.0
Cu(2)	24*g*	0.218(5)	0.023(4)	-0.023(4)	0.5
Sb	8*c*	0.271(5)	0.271(5)	0.271(5)	1.0
S(1)	2*a*	0	0	0	1.0
S(2)	24*g*	0.113(6)	0.113(6)	0.366(8)	1.0
χ^2 = 914, R_{Bragg} = 4.58, R_f = 3.18					

Table 2: Crystallographic parameters of Cu_3SbS_3 deduced from Rietveld refinement of neutron powder diffraction pattern recorded at 843 K.

Cu_3SbS_3	*Pnma* a = 7.891(1) Å, b = 10.312(1) Å, c = 6.588(1) Å				
	Site	x	y	z	Occ.
Cu(1)	8*d*	0.064(3)	0.010(2)	0.166(4)	0.37(2)
Cu(2)	8*d*	0.339(2)	0.108(2)	0.388(2)	0.47(1)
Cu(3)	8*d*	0.121(2)	0.073(2)	0.327(4)	0.51(2)
Cu(4)	4*c*	0.0805	¼	0.4585	0.09(1)
Cu(5)	4*c*	0.227	¼	0.430	0.20(1)
Sb	4*c*	0.270(1)	¼	0.889(1)	1.0
S(1)	4*c*	0.053(2)	¼	0.151(2)	1.0
S(2)	8*d*	0.172(2)	0.067(2)	0.677(3)	1.0
χ^2 = 75.5, R_{Bragg} = 3.49, R_f = 3.55					

Table 3: Crystallographic parameters of $Cu_4Sn_7S_{16}$ deduced from Rietveld refinement of neutron powder diffraction pattern recorded at 300 K.

$Cu_4Sn_7S_{16}$	$R\bar{3}m$ a = 7.362(1) Å, c = 35.965(4) Å				
	Site	x	y	z	Occ.
Cu(1)	6*c*	0	0	0.189(1)	0.5
Cu(2a)	6*c*	0	0	0.305(1)	0.4
Cu(2b)	6*c*	0	0	0.288(1)	0.6
Cu(3)	3*a*	0	0	0	1.0
Sn(1)	18*h*	0.502(1)	0.498(1)	0.251(1)	1.0
Sn(2)	3*b*	0	0	½	1.0
S(1)	18*h*	0.494(1)	0.506(1)	0.124(1)	1.0
S(2)	18*h*	0.502(1)	0.498(1)	0.375(1)	1.0
S(3)	6*c*	0	0	0.123(1)	1.0
S(4)	6*c*	0	0	0.378(1)	1.0

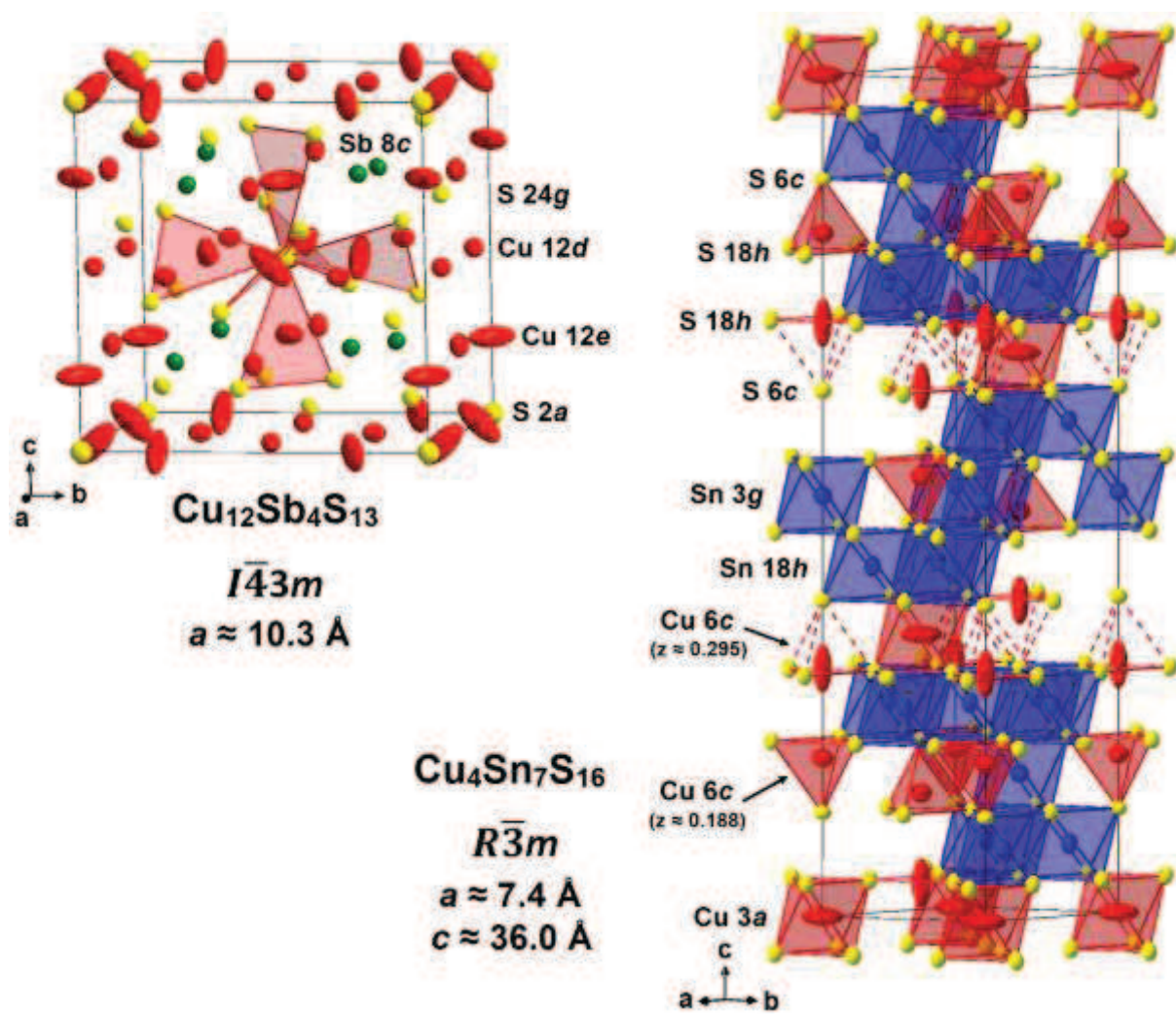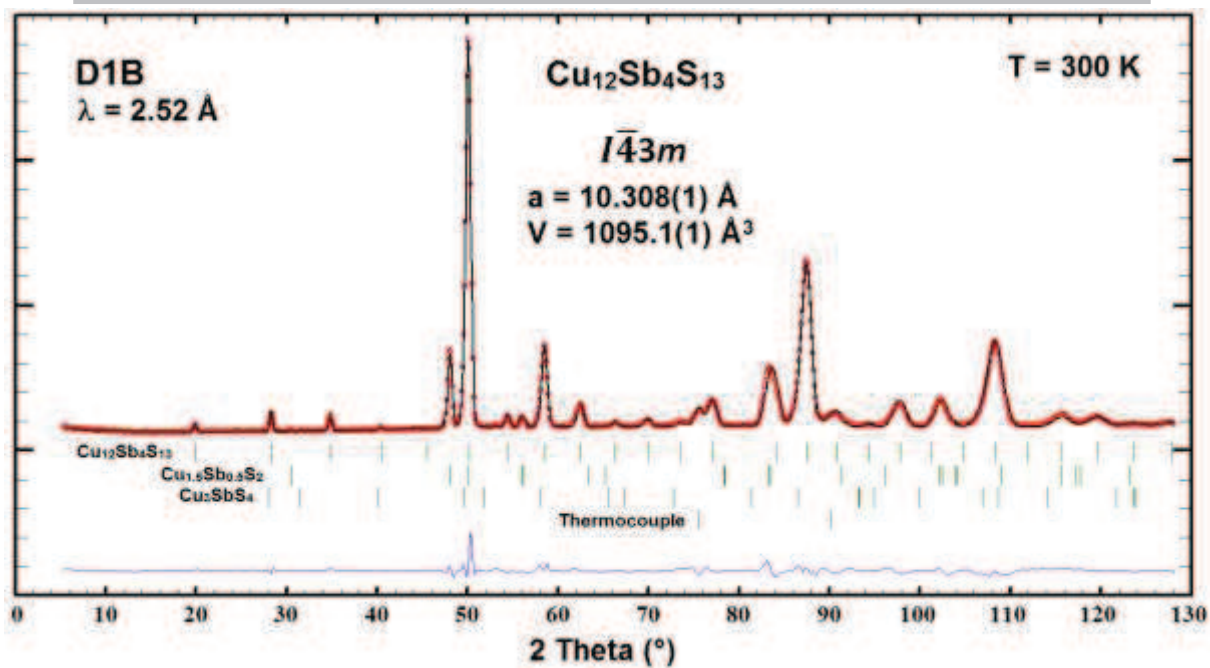$\chi^2 = 58.9$, $R_{Bragg} = 3.36$, $R_f = 3.00$

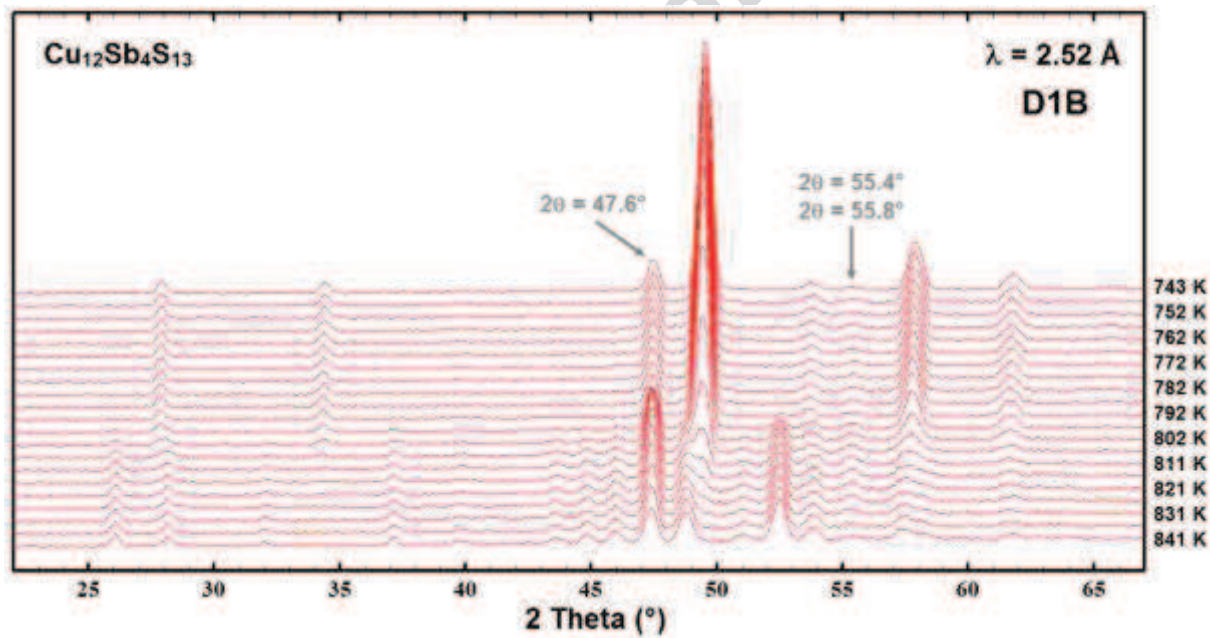**Figure 1**

Figure 2

Figure 3

Figure 4
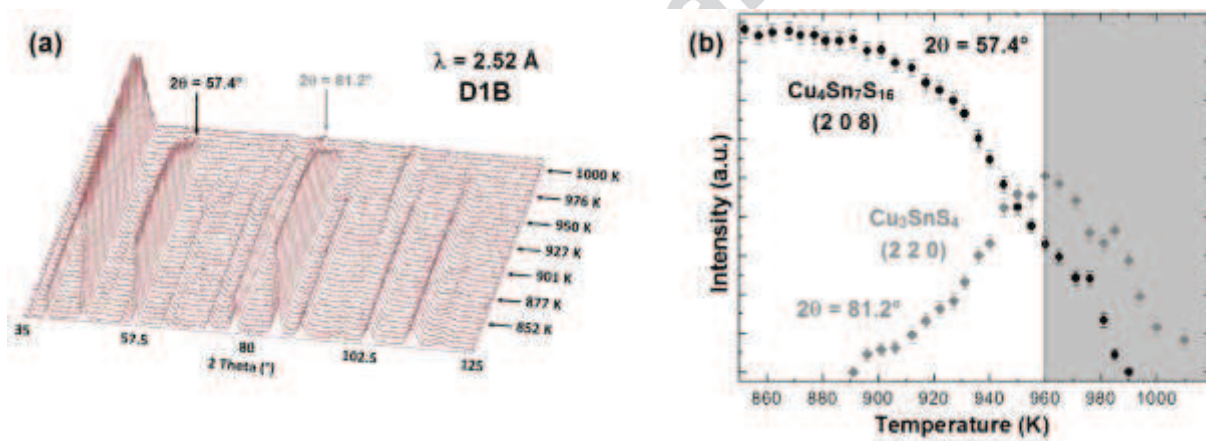
Figure 5

Figure 6

14
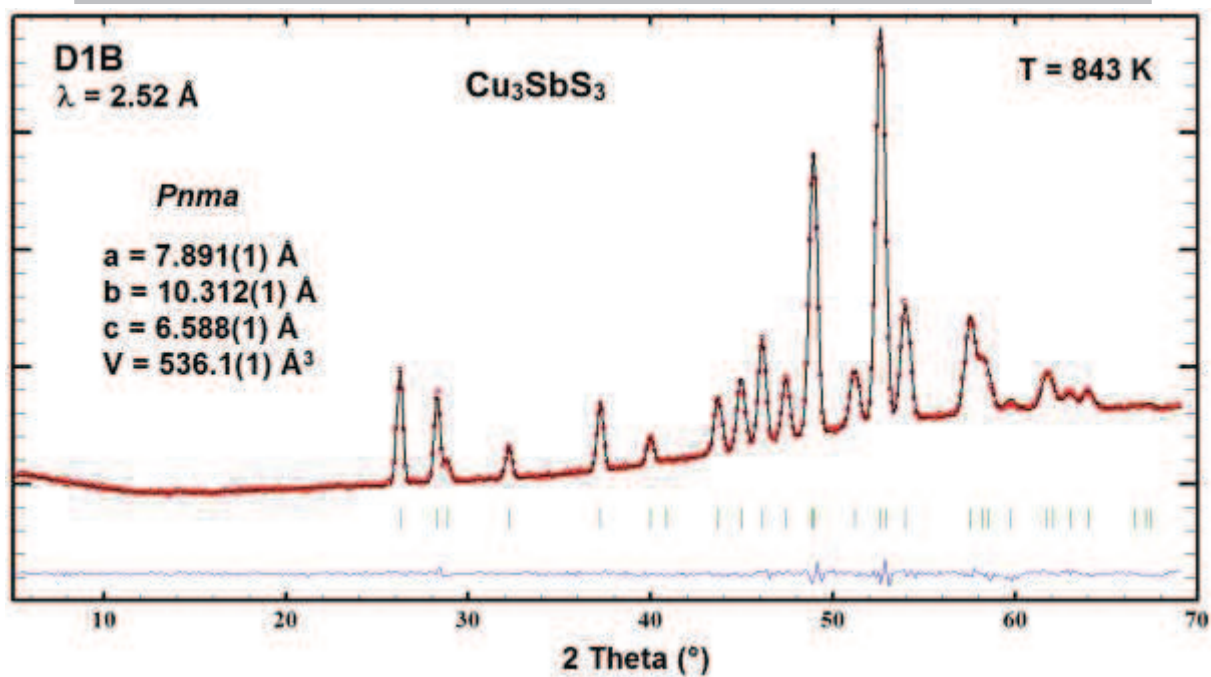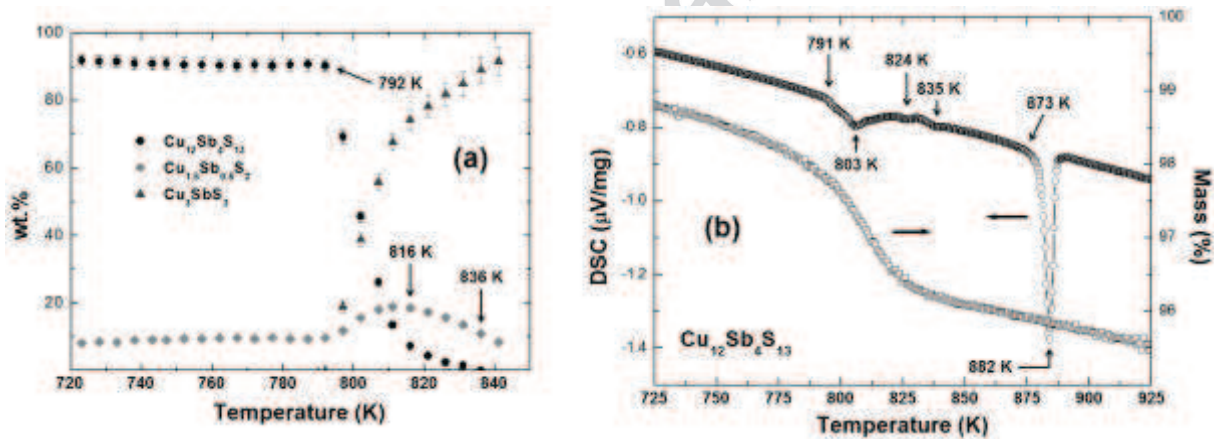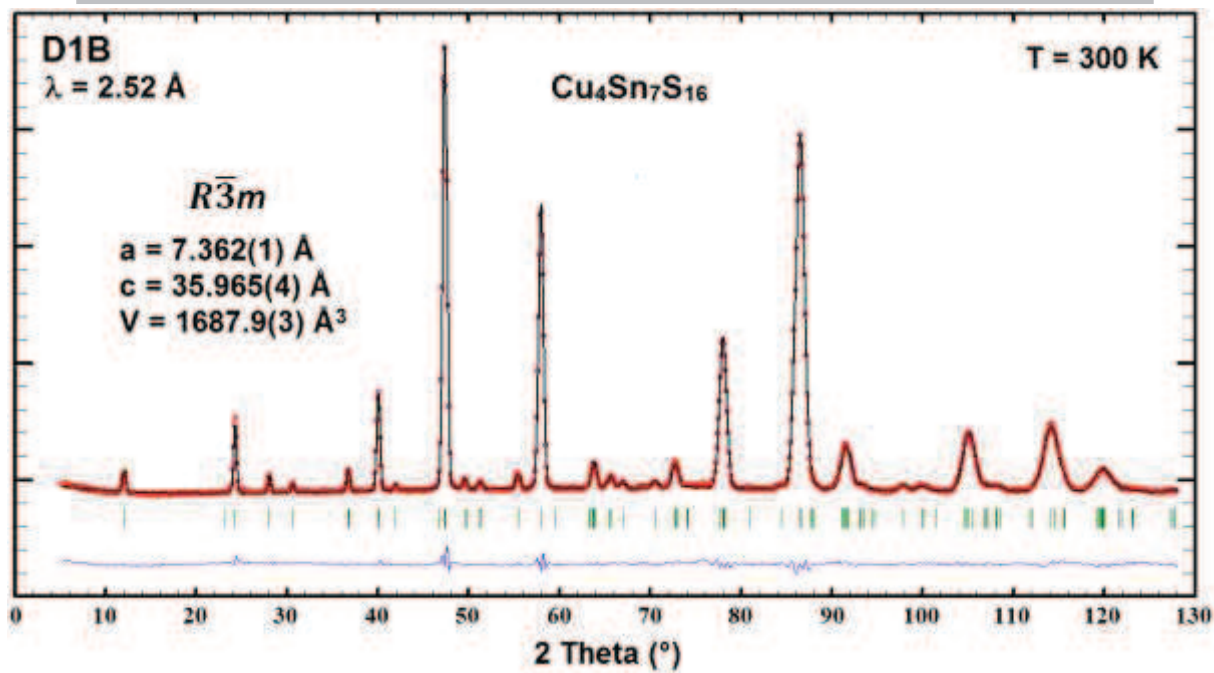
Figure 7

Figure 8

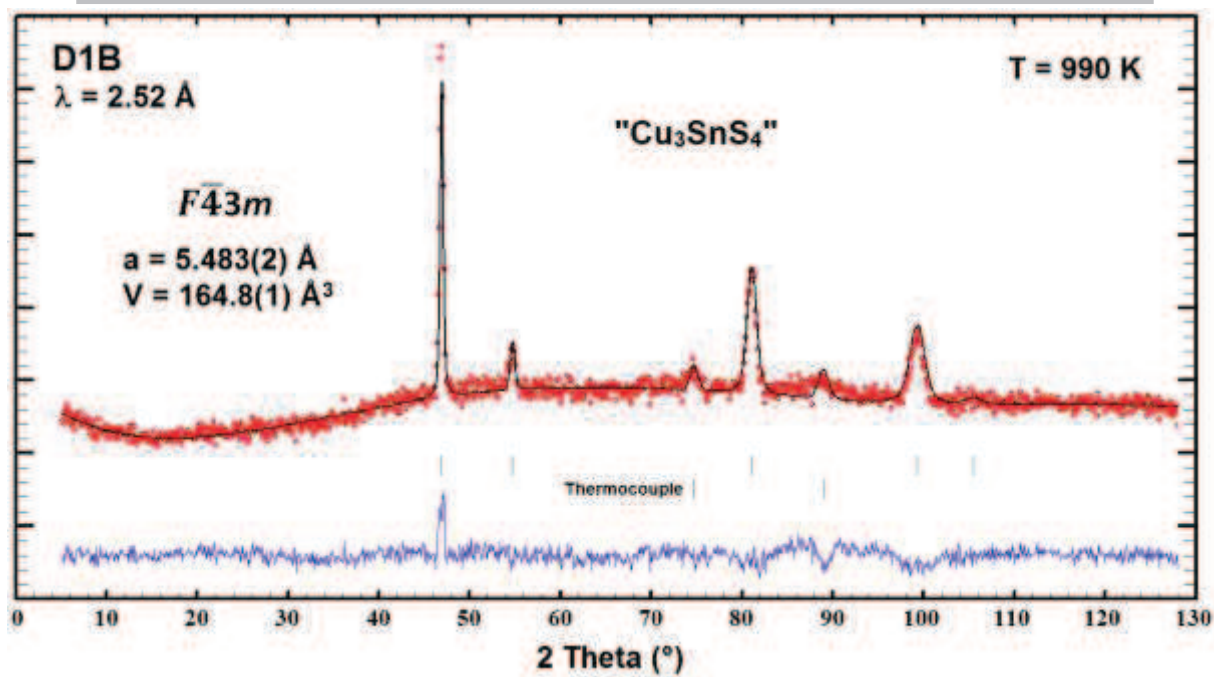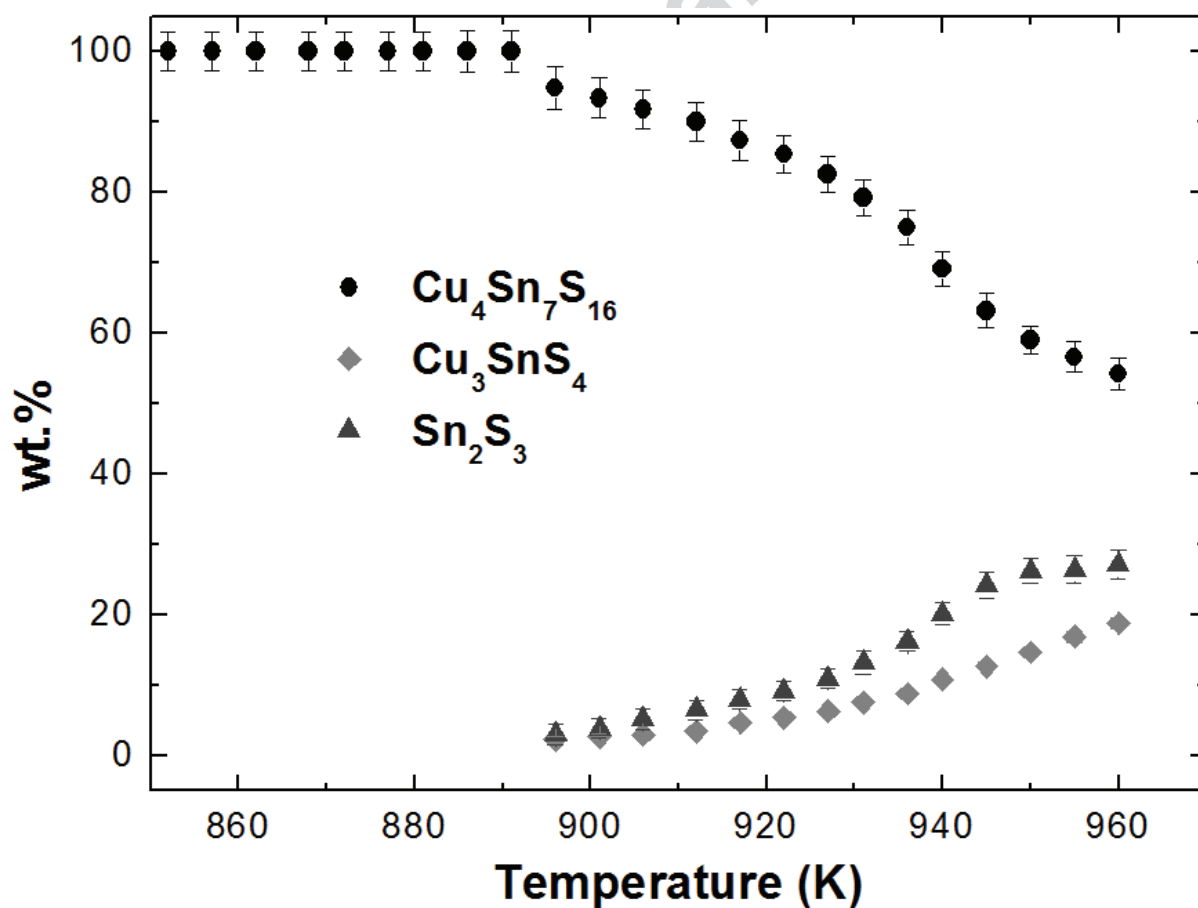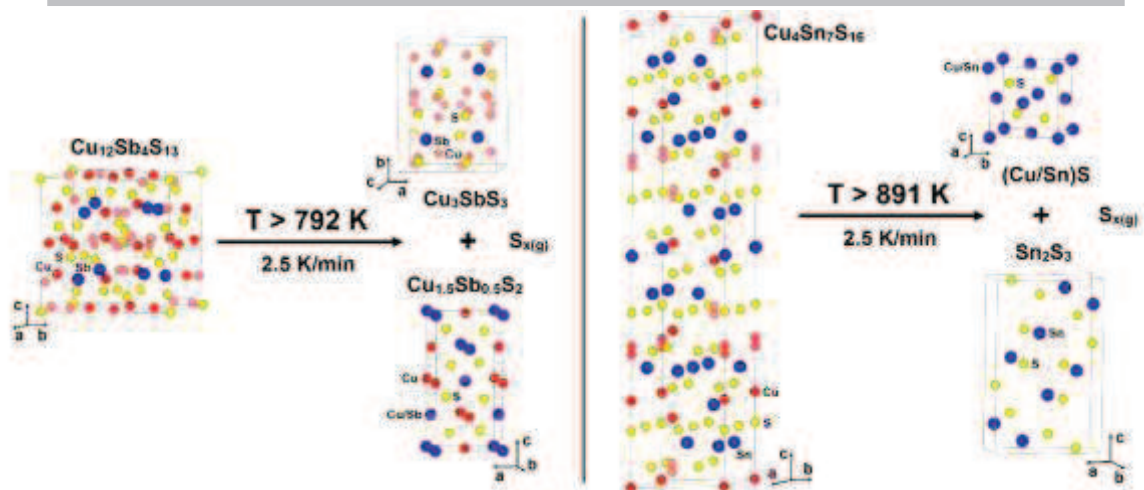**Figure 9**

In situ neutron powder diffraction data (heating rate of 2.5 K/min) indicates that (i) the ternary $Cu_{12}Sb_4S_{13}$ phase is stable up to 792 K and decomposes at higher temperature into Cu_3SbS_3 and $Cu_{1.5}Sb_{0.5}S_2$, and (ii) the $Cu_4Sn_7S_{16}$ phase is stable up to 891 K and decomposes at higher temperature into Sn_2S_3 and a cubic phase of sphalerite ZnS-type structure. Sulfur volatilization likely occurs in order to balance the overall stoichiometry.